

Optical Limiting Based on Huygens' Metasurfaces

Austin Howes,[†] Zhihua Zhu,[†] David Curie, Jason R. Avila, Virginia D. Wheeler, Richard F. Haglund, and Jason G. Valentine*

Cite This: *Nano Lett.* 2020, 20, 4638–4644

Read Online

ACCESS |

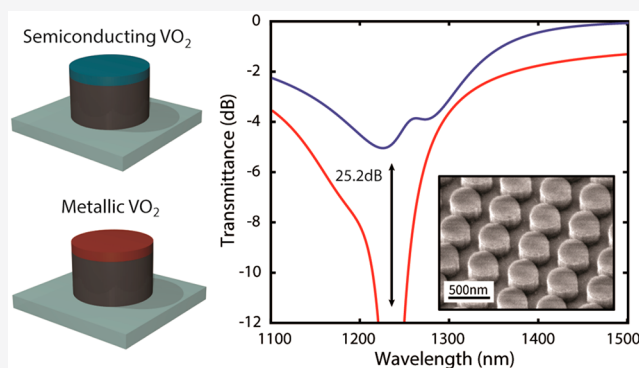
Metrics & More

Article Recommendations

Supporting Information

ABSTRACT: Optical limiting is desirable or necessary in a variety of applications that employ high-power light sources or sensitive photodetectors. However, the most prevalent methods compromise between on-state transmission and turndown ratio or rely on narrow transmission windows. We demonstrate that a metasurface-based architecture incorporating phase-change materials enables both high and broadband on-state transmission (−4.8 dB) while also providing a large turndown ratio (25.2 dB). Additionally, this design can be extended for broadband multiwavelength limiting due to the high off-resonance transmittance and readily scalable resonant wavelength. Furthermore, our choice of active material allows for protection in ultrafast laser environments due to the speed of the phase transition. These benefits offer a strong alternative to state-of-the-art optical limiters in technologies ranging from sensor protection to protective eyewear.

KEYWORDS: Huygens' metasurface, optical limiter, vanadium dioxide, phase-change material



The demand for power-limiting optics has paralleled the development of high-power lasers to mitigate damage to eyes as well as sensitive photodetectors, sensors, and cameras. For these applications, optical limiters that transmit low-intensity light (on-state) while blocking high-intensity light (off-state) are needed. In the past 20 years, many approaches for optical limiting have been investigated. The most common designs have used two-photon absorption or absorption in nonlinear media as the limiting element.^{1–5} However, many of the examined materials, such as carbon black,⁶ cadmium sulfates,⁷ graphene oxides,⁸ and silica with metal nanoparticles,⁹ have been primarily embodied in dilute liquid suspensions and suffer from turndown ratios below 10. Alternatively, some limiter designs with damage thresholds near their actuation threshold provide larger turndown ratios, albeit with the penalty of single-use protection. Whereas polymeric films¹⁰ and dye-based approaches¹¹ have high electro-optic coefficients and are less costly, they also actuate slowly and exhibit an unfavorable trade-off between the on-state transmission and turndown ratio.

The most important features for a limiter are high on-state transmission, large turndown ratio, high damage threshold, and fast response time. To passively switch from the on-state to the off-state, the limiter should incorporate a dynamic material that serves to limit the transmitted fluence once it passes a predefined threshold. Phase-change materials such as vanadium dioxide (VO₂) are well-suited for this role due to their large contrast in optical constants upon undergoing the

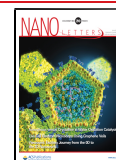
semiconductor-to-metal phase transition. This transition occurs within 60 fs when triggered optically, making the device suitable for limiting both continuous-wave as well as ultrafast pulsed lasers.¹² Additionally, the phase-transition threshold is tuned by applying stress or doping;^{13–15} therefore, the threshold intensity can be adjusted across the near-infrared depending on the application. Another candidate phase-change material is germanium antimony telluride (GST) and is often considered for tunable nanophotonic devices. However, the phase transition in GST is nonvolatile and it has lower permittivity contrast between material states than VO₂. Additionally, the transition temperature of GST is much higher than that of VO₂ and suffers greater and more rapid degradation over millions of switching cycles.^{16,17}

The growing use of nanoscale structuring in optics creates new possibilities for limiters that take advantage of resonances for increasing light–matter interaction in nearby nonlinear or tunable media. Many examples of resonant metasurfaces incorporating phase-change materials have been demonstrated for dynamic wavefront engineering,^{18–20} polarization control,²¹

Received: April 11, 2020

Revised: May 15, 2020

Published: May 18, 2020



and ultrathin optical switches.^{22–24} However, a major challenge arising from using resonances for optical limiting is that singular resonant modes are reflective and therefore limit transmission in the on-state. One strategy for overcoming these limitations to realize high on-state transmission is to use critically coupled cavity modes such as those found in Bragg cavities.²⁵ Whereas this approach can yield near-unity on-state transmission, it only does so in a narrow window that lies within a broad reflection band, severely limiting the bandwidth of the sensor.

In this work, we demonstrate a transmissive optical limiter by integrating VO₂ with a metasurface architecture that possesses overlapped optical modes. By supporting orthogonal electric and magnetic dipole Mie-type resonances at the same energy, the metasurface exhibits high, broadband transmittance in the on-state. The metasurface limits the intensity of the incident light after the VO₂ is driven through its phase transition, resulting in a change from the semiconducting to the metallic state. Moreover, an epsilon-near-zero (ENZ) mode of the VO₂ is harnessed to further decrease the transmittance in the off-state. The simulated transmission contrast between the on-state and off-state is 25.2 dB with an on-state transmission of -4.8 dB. This approach provides a superior combination of high and broadband transmittance in the on-state while preserving a large turndown ratio by exploiting optical resonances.

Dielectric resonators possess Mie-type resonances that exhibit electric and magnetic dipole-like fields^{26–28} for which the spectral position of the resonances depends on the geometry of the particle. In the case of an anisotropic resonator, such as a cylinder, the relative position of the resonances can be tuned by altering the aspect ratio (AR = diameter/height) of the resonator.^{26,29} To illustrate this concept, the transmittance spectrum of arrays of cylindrical nanoparticles are displayed in Figure 1a. Silicon is used as the dielectric due to its large refractive index and low optical loss. The dips in the blue curve correspond to the electric (E_{dp}) and magnetic (H_{dp}) dipole Mie resonances, and the fields for these modes are exhibited in Figure 1b. With the correct aspect ratio, the two modes can exist at the same energy ($\lambda_H = 1.21 \mu\text{m}$), as seen in the red curve. When this occurs for two orthogonal Mie-type resonances with equal strength, the reflected fields from one dipole mode destructively interfere with the fields of the other, resulting in zero backscattering.^{30–33} In a low-loss medium such as silicon, this corresponds to flat, near-unity transmittance, as seen in the red curve in Figure 1a. This is commonly referred to as the first Kerker condition or a Huygens' mode.^{30–32,34} Importantly, even though the transmission is flat, the surface still exhibits a strong resonance and undergoes a 2π phase shift at $\lambda_H = 1.21 \mu\text{m}$.

To transform the Huygens' metasurface into an optical limiter, a thin layer of VO₂ is added to the resonator, as seen in Figure 1d. At room temperature, VO₂ is a slightly lossy semiconductor with a large permittivity, as shown in Figure 1c. When VO₂ is heated above $\sim 67^\circ\text{C}$, it undergoes a phase change from a semiconducting, monoclinic structure to a metallic, rutile phase, resulting in a reduction in permittivity and an increase in loss, as seen in Figure 1c. In this design, optical limiting is aided by two factors. First, the metallic phase of VO₂ has a much larger imaginary component of the permittivity than the semiconducting state. This results in self-latching into an absorptive off-state when VO₂ is heated beyond its phase-transition temperature due to the absorption

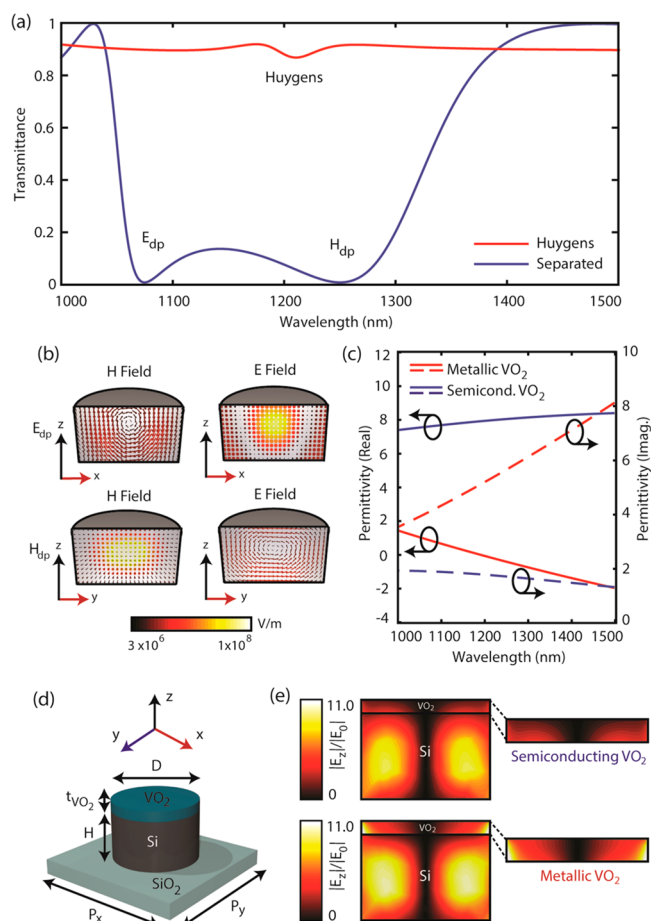


Figure 1. Dynamics of Mie resonances and integrating VO₂ into the resonator design. (a) Transmittance plots of Si resonators for metasurfaces with separated (diameter = 410 nm, height = 189 nm, and period = 656 nm) and overlapped (diameter = 438 nm, height = 189 nm, and period = 656 nm) electric and magnetic dipole Mie modes. (b) 2-D vector field plots along the middle of the resonator for the electric and magnetic dipole Mie-type resonances. (c) Real and imaginary permittivity of VO₂ in the semiconducting and metallic states. (d) Unit-cell design of the VO₂-integrated metasurface. (e) Z-oriented cross sections displaying the electric field distribution for the VO₂-integrated resonator design in the metallic and semiconductor states.

of the incident radiation. Second, we have engineered the Huygens' resonance to coincide with the ENZ point when VO₂ is in the metallic state. As the permittivity of VO₂ approaches zero, the electric field inside VO₂ is enhanced due to the continuity of the normal displacement field, as illustrated in Figure 1e. In the case of metallic VO₂, the electric field inside the VO₂ layer is enhanced up to a factor of 11 compared with the field inside the silicon resonator. This field enhancement results in increased absorption, given by $A = \int \epsilon_i |E|^2 dV$, and produces a large turndown ratio.

To maximize the on-state transmission and turndown ratio, the two Mie dipole-type resonances in the Si resonator must achieve a perfect spectral overlap. In Figure 2a,b, the transmittance of the VO₂ integrated metasurface is plotted as a function of aspect ratio. For large aspect ratios (AR > 2.6), the magnetic and electric dipole Mie resonances are spectrally separated. As the aspect ratio approaches AR = 2.5, the two resonances merge and destructively interfere, resulting in high transmittance (-4.8 dB) at $\lambda_H = 1.24 \mu\text{m}$ in the semi-

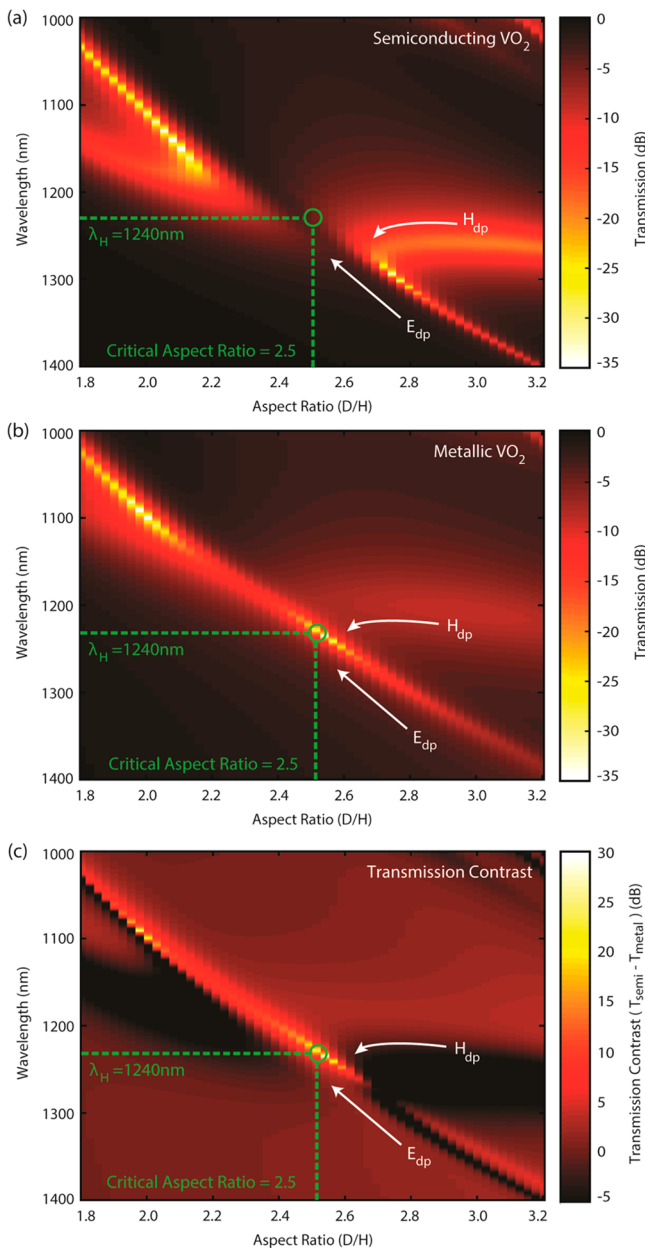


Figure 2. Engineering overlapped Mie resonances and optimizing optical contrast between the on-state and off-state. Transmittance as a function of wavelength and aspect ratio (diameter/height) for VO_2 -integrated Huygens' metasurfaces when in the (a) on-state and (b) off-state. (c) Transmission contrast as a function of wavelength and aspect ratio. The optimized metasurface geometry ($t_{\text{Si}} = 190$ nm, AR = 2.5, $P_x = P_y = 660$ nm, $t_{\text{VO}_2} = 35$ nm) exhibits maximum optical contrast and minimum off-state transmittance.

conducting state (Figure 2a). In the metallic state (Figure 2b), VO_2 is near the ENZ point at λ_{H} , reducing the transmittance to -30.0 dB and yielding a design with a modulation depth of 25.2 dB, as illustrated in Figure 2c.

To validate this approach, we fabricated and characterized devices with geometries supporting the maximum turn-down ratio ($t_{\text{Si}} = 190$ nm, $D = 475$ nm, $P_x = P_y = 660$ nm, and $t_{\text{VO}_2} = 35$ nm). The simulated on-state and off-state transmittances are illustrated in Figure 3a. The metasurfaces were created by starting with a 190 nm silicon device layer, grown on a SiO_2 wafer using plasma-enhanced chemical vapor deposition. VO_2

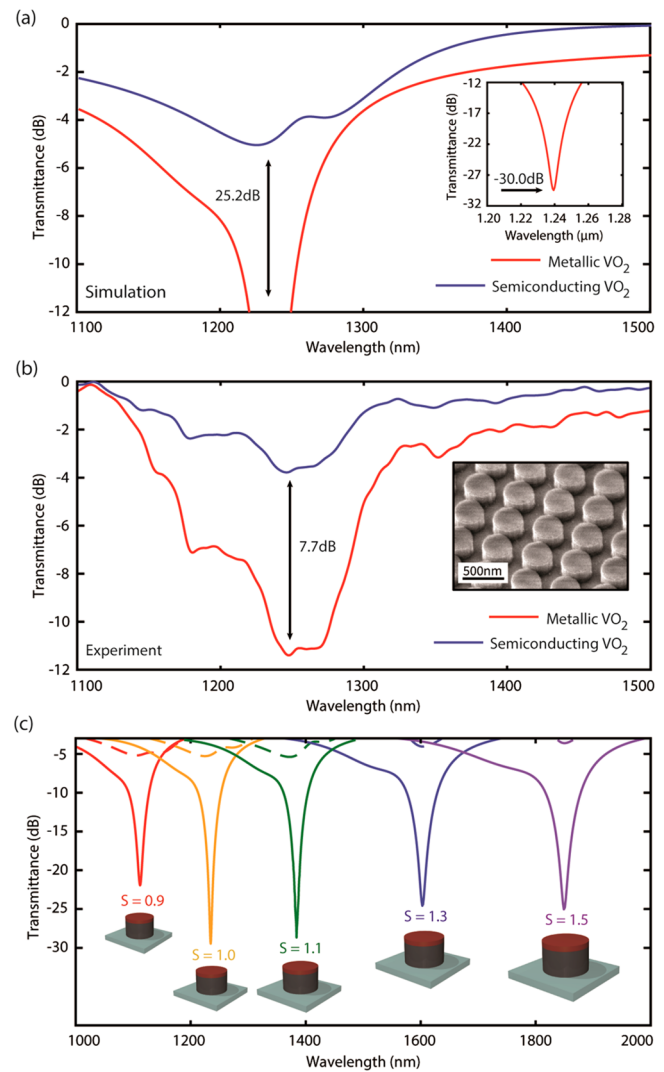


Figure 3. Experimental demonstration of VO_2 -integrated metasurface-based optical limiter. (a) Simulated and (b) experimental transmittance of the limiter with $t_{\text{Si}} = 190$ nm, $D = 475$ nm, $P_x = P_y = 660$ nm, and $t_{\text{VO}_2} = 35$ nm in the on and off-states. (b, inset) SEM image of the fabricated device. (c) Simulated transmission spectra in the on- (dashed) and off-states (solid) for several optimized metasurface designs with scaled dimensions ($S = 0.9, 1.1, 1.3,$ and 1.5), where the diameter, period, and resonator height are all multiplied by S .

was deposited on top of the wafer using atomic layer deposition (ALD). The resonator structures were formed using electron beam lithography (EBL) and reactive ion etching (RIE) with an aluminum oxide etch mask. A scanning electron micrograph (SEM) of the fabricated metasurface is pictured in Figure 3b. To create a symmetric environment around the resonator, which helps with impedance matching, PMMA was spun on top of the completed metasurface. A more detailed description of the fabrication process is included in the Methods section.

The experimental transmittance data are plotted in Figure 3b for a metasurface with an operating wavelength of $\lambda_{\text{H}} = 1.24$ μm . To switch between the on-state and off-state, a resistive heater was used to modulate the metasurface temperature between 25 (on-state) and 85° (off-state). In the on-state, the transmittance closely matches the simulated performance with a transmittance of -4.8 dB at λ_{H} . In the off-state, the minimum

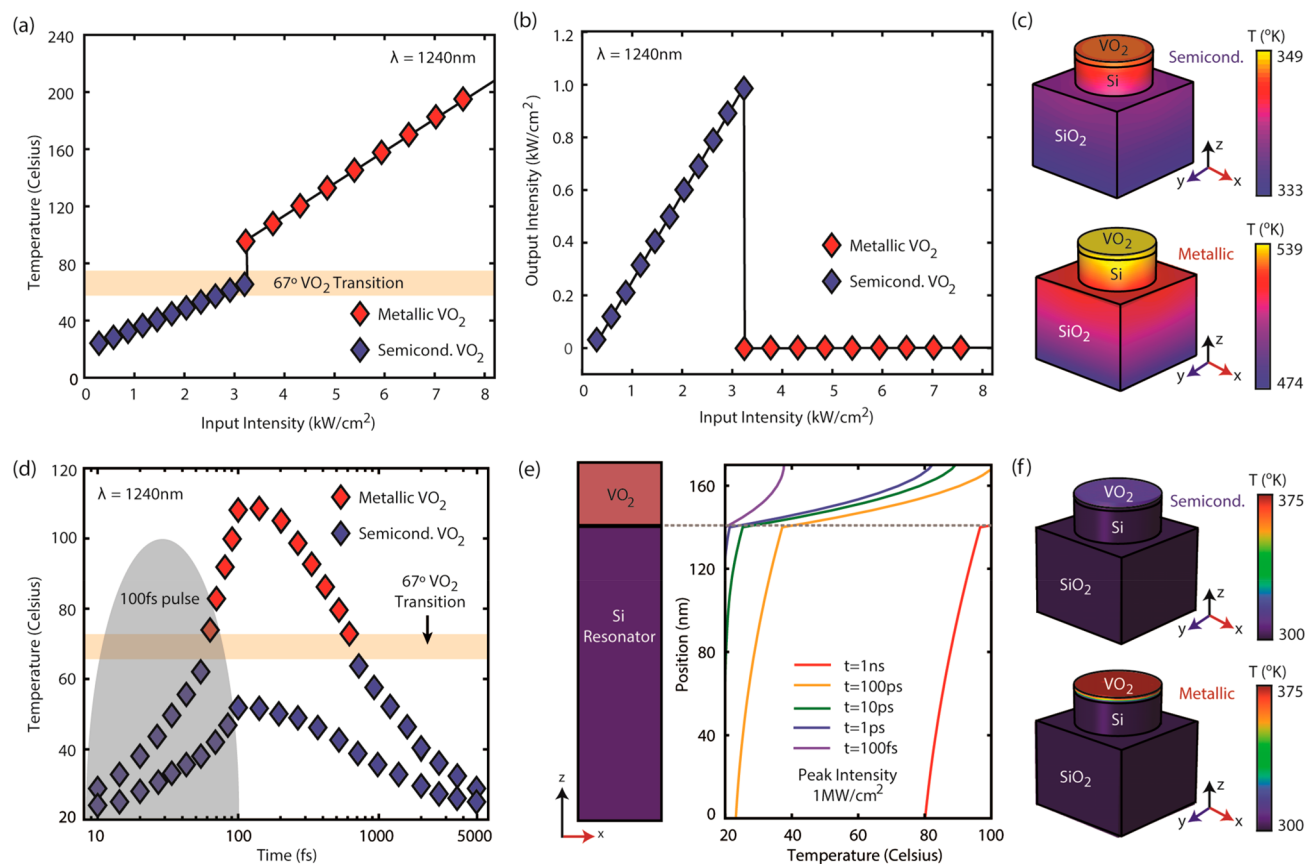


Figure 4. Thermal performance of VO₂ and its effect on optical limiting functionality. (a) Simulated mean temperature of the VO₂ film as a function of incident intensity in a steady-state environment. (b) Nonlinear relationship between the output intensity and input intensity, demonstrating the optical limiting behavior. (c) Thermal distribution of the metasurface unit cell when operating in the on-state (input intensity = 3.1 kW/cm²) and off-state (input intensity = 9.0 kW/cm²). (d) Temporal thermal characteristics of the optical limiter for two 100 fs pulses of peak intensities of 2 and 5 MW/cm². The higher the incident intensity, the longer the recovery time due to heat dissipation. (e) Heat confinement as a function of pulse duration. The position on the *y* axis corresponds to the *z* axis of the resonator structure, as seen on the left. (f) Thermal distribution of the metasurface unit cell when operating in the on-state and off-state with a pulsed excitation.

transmittance achieved is -11.7 dB, resulting in a modulation depth of 7.7 dB. The discrepancy between simulated and experimental results in the off-state might stem from several factors. First, the metasurface design relies on the spectral overlap of the Huygens' point of the resonator and the ENZ point of the metallic-state VO₂, and even small fabrication errors can result in spectral misalignment. Second, the permittivity function of VO₂ is sensitive to stress in the film, and its switching behavior is highly dependent on its environment.³⁵ At 35 nm thickness, the VO₂ is not a completely continuous film, and only certain regions of VO₂ may be completely switching. The *z*-oriented fields from the modes in the silicon resonator are strongest near the outer edges (Figure 1b,e); therefore, the enhanced absorption is strongest in these areas. Finally, the noncontinuous VO₂ film results in additional scattering, leading to a broader resonance, as illustrated in Figure 3b.

A particular advantage of this design is that the working wavelength can be adjusted by tuning the size of the resonators. Whereas the ENZ wavelength of VO₂ is fixed, it still exhibits a large permittivity and absorption contrast between the semiconducting and metallic states away from the ENZ point. To explore how this type of metasurface operates at other wavelengths, we simulated devices with unit-cell dimensions uniformly scaled by a factor *S*, with the exception

that the VO₂ thickness was held constant. For *S* = 0.9, 1.1, 1.3, and 1.5, the resonant wavelengths of the Huygens' modes are 1060, 1400, 1610, and 1870 nm, as pictured in Figure 3c. A modulation depth of >18 dB is observed for all four metasurfaces compared with 25.2 dB for a device with *S* = 1. Thus whereas spectral overlap with the ENZ point is advantageous, a large modulation depth can still be achieved away from this condition, allowing the design to be employed for a wide range of laser wavelengths.

It is also important to investigate the thermal dynamics of the metasurface to estimate the limiting threshold. To characterize the performance of the limiter design, a finite-difference solver (CST Microwave Studio) is used to calculate the mean temperature of the VO₂ film using material properties provided in Supplementary Table 1. The absorbed power is assumed to take place entirely within the VO₂ layer due to the negligible losses of silicon and SiO₂ and is defined by $Q = AI_{\text{in}}\alpha$, where *A* is the cross-sectional area of the unit cell, *I*_{in} is the incident intensity, and α is the absorptance of the metasurface. The absorptances of the semiconducting and metallic VO₂ states at $\lambda = 1240$ nm are $\alpha_{\text{semi}} = 0.6$ and $\alpha_{\text{metal}} = 0.97$. These parameters govern the temperature of the film as a function of the input intensity, as illustrated in Figure 4a,c. The VO₂ film in the model is treated as the heat source, and the resonator is surrounded by air with a convective heat transfer

coefficient of $50 \text{ W/m}^2 \text{ K}$. Adiabatic boundary conditions are used in the in-plane direction to mimic an infinite array. On the basis of these parameters, the incident intensity needed to heat the VO_2 to its phase-transition temperature of 67°C is 3.2 kW/cm^2 (Figure 4a,b). For context, the damage threshold of the human cornea in the near-IR is $\sim 0.1 \text{ W/cm}^2$. This result suggests that our limiter design can be better applied in high-power laser applications such as material processing or medical equipment than for eye protection. However, the limiting threshold can be decreased by adjusting the Huygens' mode wavelength of the resonator and harnessing the large VO_2 absorption at shorter wavelengths.

In addition to steady-state analysis, the transient behavior of the limiter is also important because many laser sources that are most relevant for optimal limiting applications are pulsed. In this case, critical parameters include the response time as well as the recovery time for pulsed sources. Because the energy is being absorbed in a much shorter time, the intensity needed to switch the metasurface is significantly higher than that in Figure 4a–c. For example, for a pulse lasting 100 fs, a peak intensity of 2 MW/cm^2 will raise the temperature of VO_2 to only 50°C and will not trigger the limiting behavior, whereas a pulse of 5 MW/cm^2 will force the VO_2 above 100°C . As expected, the relaxation time for the device depends on the maximum temperature reached during the duration of the pulse. In the case of a 5 MW/cm^2 100 fs pulse, the system cools to the semiconducting state within $\sim 1 \text{ ps}$, as seen in Figure 4d. The small thermal mass of the VO_2 and the relatively high thermal diffusivity of the silicon structure result in a short thermal relaxation time, mitigating heat accumulation and damage to the film.³⁶

We can better understand the response of the resonator– VO_2 system by observing its evolution from pulsed to continuous-wave exposure. For example, in the case of excitation via an ultrafast (100 fs) pulse, nearly all of the thermal energy is contained within the VO_2 layer, as seen in Figure 4f. This is a consequence of the thermal conductivity of Si and short time scales compared with the steady-state solutions (Figure 4c). We can understand how the pulse duration affects the maximum temperature and thermal distribution within the metasurface structure by plotting the temperature as a function of position after exposure to pulses of various time scales. Whereas increasing the pulse duration increases the average temperature of the device, in particular, the VO_2 layer, it also allows more energy to bleed into the underlying Si resonator, as shown in Figure 4e. As the length of exposure is increased beyond the picosecond time scale, we begin to see the thermal behavior of the system converge to the steady-state profile in Figure 4c. This provides a more complete picture of the response of this metasurface limiter in different application spaces depending on the allowed intensities and damage threshold of the device.

In summary, we have created a metasurface-based optical limiter with large and broadband on-state transmittance while also maintaining a large turndown ratio. This is achieved by harnessing overlapped optical resonances, or Huygens' modes, in dielectric resonators into which a thin film of VO_2 has been integrated. The use of VO_2 as the active component allows for protection from ultrafast lasers due to the speed of the insulator–metal transition. Because of the broad transmission band, several of these films could be layered to cover a wide range of laser wavelengths from the near- to the far-infrared regime.

METHODS

Thin (35 nm) VO_2 films were grown on the silicon device layer via ALD and annealed.³⁷ The resonator structure was defined by a standard electron-beam lithography protocol with PMMA as the photoresist and 1:3 MIBK/IPA as the developing agent. Afterward, a 55 nm Al_2O_3 etch mask was prepared by electron beam deposition, and the sample was placed in hot Remover PG until the undeveloped PMMA was successfully lifted off the sample. The samples were then treated with a 1:8 30% $\text{H}_2\text{O}_2/\text{H}_2\text{O}$ solution for 15 min at 85°C to selectively etch the VO_2 that was not underneath the hard mask. The samples were then formed using RIE to define the silicon cylinders. Finally, a top coat of PMMA was applied and baked at 180°C for 3 min to protect the metasurface layer and create an index match to the SiO_2 substrate to prevent unwanted reflection during measurements.

ASSOCIATED CONTENT

Supporting Information

The Supporting Information is available free of charge at <https://pubs.acs.org/doi/10.1021/acs.nanolett.0c01574>.

Thermal properties of materials in the Huygens' metasurface-based optical limiter design (PDF)

AUTHOR INFORMATION

Corresponding Author

Jason G. Valentine – Department of Mechanical Engineering, Vanderbilt University, Nashville, Tennessee 37212, United States; orcid.org/0000-0001-9943-7170; Email: jason.g.valentine@vanderbilt.edu

Authors

Austin Howes – Department of Physics and Astronomy, Vanderbilt University, Nashville, Tennessee 37212, United States

Zhihua Zhu – Department of Electrical Engineering and Computer Science, Vanderbilt University, Nashville, Tennessee 37212, United States

David Curie – Department of Physics and Astronomy, Vanderbilt University, Nashville, Tennessee 37212, United States

Jason R. Avila – U.S. Naval Research Laboratory, Washington, District of Columbia 20375, United States

Virginia D. Wheeler – U.S. Naval Research Laboratory, Washington, District of Columbia 20375, United States; orcid.org/0000-0002-6024-9516

Richard F. Haglund – Department of Physics and Astronomy, Vanderbilt University, Nashville, Tennessee 37212, United States; orcid.org/0000-0002-2701-1768

Complete contact information is available at: <https://pubs.acs.org/doi/10.1021/acs.nanolett.0c01574>

Author Contributions

[†]A.H. and Z.Z. contributed equally to the work. A.H. and Z.Z. performed the simulation work, sample fabrication, and measurements. D.C. assisted in the fabrication of devices. J.R.A. and V.D.W. provided the VO_2 samples. R.F.H. and J.G.V. designed and oversaw the study and provided equipment for the measurements. R.F.H. and J.G.V. assisted A.H. in editing the manuscript.

Notes

The authors declare no competing financial interest.

ACKNOWLEDGMENTS

A.H., Z.Z., and J.G.V. acknowledge support from the National Science Foundation (NSF) under grant DMR-1610357 as well as support from the Northrop Grumman Corporation. R.F.H. and Z.Z. acknowledge support from the U.S. Department of Energy under grant DE-FG02-01ER45916. V.D.W. and J.R.A. acknowledge support from the Office of Naval Research (ONR) and the American Society for Engineering Education (ASEE).

REFERENCES

- (1) Karimzadeh, R.; Aleali, H.; Mansour, N. Thermal Nonlinear Refraction Properties of Ag₂S Semiconductor Nanocrystals with Its Application as a Low Power Optical Limiter. *Opt. Commun.* **2011**, *284* (9), 2370–2375.
- (2) Westlund, R.; Glimsdal, E.; Lindgren, M.; Vestberg, R.; Hawker, C.; Lopes, C.; Malmström, E. Click Chemistry for Photonic Applications: Triazole-Functionalized Platinum(II) Acetylides for Optical Power Limiting. *J. Mater. Chem.* **2008**, *18* (2), 166–175.
- (3) Ehrlich, J. E.; Wu, X. L.; Lee, I.-Y. S.; Hu, Z.-Y.; Röckel, H.; Marder, S. R.; Perry, J. W. Two-Photon Absorption and Broadband Optical Limiting with Bis-Donor Stilbenes. *Opt. Lett.* **1997**, *22* (24), 1843.
- (4) He, G. S.; Reinhardt, B. A.; Bhatt, J. C.; Dillard, A. G.; McKellar, R.; Xu, C.; Prasad, P. N. Two-Photon Absorption and Optical-Limiting Properties of Novel Organic Compounds: Erratum. *Opt. Lett.* **1995**, *20* (18), 1930.
- (5) Kannan, R.; He, G. S.; Lin, T. C.; Prasad, P. N.; Vaia, R. A.; Tan, L. S. Toward Highly Active Two-Photon Absorbing Liquids. Synthesis and Characterization of 1,3,5-Triazine-Based Octupolar Molecules. *Chem. Mater.* **2004**, *16* (1), 185–194.
- (6) Jin, M. H.; Durstock, M.; Dai, L. *Carbon Nanotechnology: Developments in Chemistry, Physics, Materials Science and Device Applications*; Elsevier B.V., 2006; pp 611–631.
- (7) Dhanuskodi, S.; Girisun, T. C. S.; Smijesh, N.; Philip, R. Two-Photon Absorption and Optical Limiting in Trithiourea Cadmium Sulphate. *Chem. Phys. Lett.* **2010**, *486*, 80–83.
- (8) Liaros, N.; Koudoumas, E.; Couris, S. Broadband near Infrared Optical Power Limiting of Few Layered Graphene Oxides. *Appl. Phys. Lett.* **2014**, *104* (19), 191112.
- (9) Du, Z.; Chen, L.; Kao, T. S.; Wu, M.; Hong, M. Improved Optical Limiting Performance of Laser-Ablation-Generated Metal Nanoparticles Due to Silica-Microsphere-Induced Local Field Enhancement. *Beilstein J. Nanotechnol.* **2015**, *6* (1), 1199–1204.
- (10) Ali, H. E. A Novel Optical Limiter and UV-Visible Filters Made of Poly (Vinyl Alcohol)/KMnO₄ Polymeric Films on Glass-Based Substrate. *J. Mater. Sci.: Mater. Electron.* **2019**, *30* (7), 7043–7053.
- (11) Liu, H.-K. Nonlinear Optical Limiting of the Azo Dye Methyl-Red Doped Nematic Liquid Crystalline Films. *Opt. Eng.* **2003**, *42* (10), 2936.
- (12) Jager, M. F.; Ott, C.; Kraus, P. M.; Kaplan, C. J.; Pouse, W.; Marvel, R. E.; Haglund, R. F.; Neumark, D. M.; Leone, S. R. Tracking the Insulator-to-Metal Phase Transition in VO₂ with Few-Femtosecond Extreme UV Transient Absorption Spectroscopy. *Proc. Natl. Acad. Sci. U. S. A.* **2017**, *114* (36), 9558–9563.
- (13) Chen, X.; Wu, M.; Liu, X.; Wang, D.; Liu, F.; Chen, Y.; Yi, F.; Huang, W.; Wang, S. Tuning the Doping Ratio and Phase Transition Temperature of VO₂ Thin Film by Dual-Target Co-Sputtering. *Nanomaterials* **2019**, *9* (6), 834.
- (14) Jin, P.; Nakao, S.; Tanemura, S. Tungsten Doping into Vanadium Dioxide Thermochromic Films by High-Energy Ion Implantation and Thermal Annealing. *Thin Solid Films* **1998**, *324* (1–2), 151–158.
- (15) Atkin, J. M.; Berweger, S.; Chavez, E. K.; Raschke, M. B.; Cao, J.; Fan, W.; Wu, J. Strain and Temperature Dependence of the Insulating Phases of VO₂ near the Metal-Insulator Transition. *Phys. Rev. B: Condens. Matter Mater. Phys.* **2012**, *85* (2), 1–4.
- (16) Crunteanu, A.; Givernaud, J.; Leroy, J.; Mardivirin, D.; Champeaux, C.; Orlianges, J. C.; Catherinot, A.; Blondy, P. Voltage- and Current-Activated Metal-Insulator Transition in VO₂-Based Electrical Switches: A Lifetime Operation Analysis. *Sci. Technol. Adv. Mater.* **2010**, *11* (6), 065002.
- (17) Kolobov, A. V.; Fons, P.; Frenkel, A. I.; Ankudinov, A. L.; Tominaga, J.; Uruga, T. Understanding the Phase-Change Mechanism of Rewritable Optical Media. *Nat. Mater.* **2004**, *3* (10), 703–708.
- (18) Kim, M.; Jeong, J.; Poon, J. K. S.; Eleftheriades, G. V. Vanadium-Dioxide-Assisted Digital Optical Metasurfaces for Dynamic Wavefront Engineering. *J. Opt. Soc. Am. B* **2016**, *33* (5), 980.
- (19) Forouzmand, A.; Mosallaei, H. Dynamic Beam Control via Mie-Resonance Based Phase-Change Metasurface: A Theoretical Investigation. *Opt. Express* **2018**, *26* (14), 17948.
- (20) Yin, X.; Steinle, T.; Huang, L.; Taubner, T.; Wuttig, M.; Zentgraf, T.; Giessen, H. Beam Switching and Bifocal Zoom Lensing Using Active Plasmonic Metasurfaces. *Light: Sci. Appl.* **2017**, *6* (7), No. e17016.
- (21) Peng, X. Y.; Wang, B.; Teng, J.; Kana Kana, J. B.; Zhang, X. Active near Infrared Linear Polarizer Based on VO₂ Phase Transition. *J. Appl. Phys.* **2013**, *114* (16), 163103.
- (22) Zhu, Z.; Evans, P. G.; Haglund, R. F.; Valentine, J. G. Dynamically Reconfigurable Metadevice Employing Nanostructured Phase-Change Materials. *Nano Lett.* **2017**, *17* (8), 4881–4885.
- (23) Gholipour, B.; Karvounis, A.; Yin, J.; Soci, C.; MacDonald, K. F.; Zheludev, N. I. Phase-Change-Driven Dielectric-Plasmonic Transitions in Chalcogenide Metasurfaces. *NPG Asia Mater.* **2018**, *10* (6), 533–539.
- (24) Kats, M. A.; Sharma, D.; Lin, J.; Genevet, P.; Blanchard, R.; Yang, Z.; Qazilbash, M. M.; Basov, D. N.; Ramanathan, S.; Capasso, F. Ultra-Thin Perfect Absorber Employing a Tunable Phase Change Material. *Appl. Phys. Lett.* **2012**, *101* (22), 221101.
- (25) Vella, J. H.; Goldsmith, J. H.; Browning, A. T.; Limberopoulos, N. I.; Vitebskiy, I.; Makri, E.; Kottos, T. Experimental Realization of a Reflective Optical Limiter. *Phys. Rev. Appl.* **2016**, *5* (6), 1–7.
- (26) Evlyukhin, A. B.; Novikov, U.; Zywiets, R.; Eriksen, C.; Reinhardt, S.; Bozhevolnyi, B. C.; Chichkov, B. N. Demonstration of Magnetic Dipole Resonances of Dielectric Nanospheres in the Visible Region. *Nano Lett.* **2012**, *12* (7), 3749–3755.
- (27) Staude, I.; Miroshnichenko, A. E.; Decker, M.; Fofang, N. T.; Liu, S.; Gonzales, E.; Dominguez, J.; Luk, T. S.; Neshev, D. N.; Brener, I.; Kivshar, Y. Tailoring Directional Scattering through Magnetic and Electric Resonances in Subwavelength Silicon Nanodisks. *ACS Nano* **2013**, *7* (9), 7824–7832.
- (28) Kuznetsov, A. I.; Miroshnichenko, A. E.; Fu, Y. H.; Zhang, J.; Luk'yanchuk, B. Magnetic Light. *Sci. Rep.* **2012**, *2*, 1–6.
- (29) Bezares, F. J.; Long, J. P.; Glembocki, O. J.; Guo, J.; Rendell, R. W.; Kasica, R.; Shirey, L.; Owrutsky, J. C.; Caldwell, J. D. Mie Resonance-Enhanced Light Absorption in Periodic Silicon Nanopillar Arrays. *Opt. Express* **2013**, *21* (23), 27587.
- (30) Monticone, F.; Estakhri, N. M.; Alù, A. Full Control of Nanoscale Optical Transmission with a Composite Metascreen. *Phys. Rev. Lett.* **2013**, *110* (20), 1–5.
- (31) Pfeiffer, C.; Grbic, A. Metamaterial Huygens' Surfaces: Tailoring Wave Fronts with Reflectionless Sheets. *Phys. Rev. Lett.* **2013**, *110* (19), 1–5.
- (32) Pfeiffer, C.; Emani, N. K.; Shaltout, A. M.; Boltasseva, A.; Shalae, V. M.; Grbic, A. Efficient Light Bending with Isotropic Metamaterial Huygens' Surfaces. *Nano Lett.* **2014**, *14* (5), 2491–2497.
- (33) Decker, M.; Staude, I.; Falkner, M.; Dominguez, J.; Neshev, D. N.; Brener, I.; Pertsch, T.; Kivshar, Y. S. High-Efficiency Dielectric Huygens' Surfaces. *Adv. Opt. Mater.* **2015**, *3* (6), 813–820.
- (34) Howes, A.; Wang, W.; Kravchenko, I.; Valentine, J. Dynamic Transmission Control Based on All-Dielectric Huygens Metasurfaces. *Optica* **2018**, *5* (7), 787.
- (35) Braun, J. M.; Schneider, H.; Helm, M.; Mirek, R.; Boatner, L. A.; Marvel, R. E.; Haglund, R. F.; Pashkin, A. Ultrafast Response of

Photoexcited Carriers in VO₂ at High-Pressure. *New J. Phys.* **2018**, *20* (8), 083003.

(36) Oh, D. W.; Ko, C.; Ramanathan, S.; Cahill, D. G. Thermal Conductivity and Dynamic Heat Capacity across the Metal-Insulator Transition in Thin Film VO₂. *Appl. Phys. Lett.* **2010**, *96* (15), 151906.

(37) Kozen, A. C.; Joress, H.; Currie, M.; Anderson, V. R.; Eddy, C. R.; Wheeler, V. D. Structural Characterization of Atomic Layer Deposited Vanadium Dioxide. *J. Phys. Chem. C* **2017**, *121* (35), 19341–19347.